Sliding Mode Based Combined Speed and Direct Thrust Force Control of Linear Permanent Magnet Synchronous Motors With First-Order Plus Integral Sliding Condition

Muhammad Ali Masood Cheema, *Member, IEEE*, John Edward Fletcher, *Senior Member, IEEE*, Mohammad Farshadnia, *Member, IEEE*, and Muhammad Faz Rahman, *Fellow, IEEE*

***Abstract*—A combined speed and direct thrust force control scheme in the synchronously rotating stator flux oriented reference frame based on sliding mode control is proposed for a linear permanent magnet synchronous motor. First-order stator flux dynamics and a second-order nonlinear state-space model for the combined dynamics of speed and thrust force as system states are presented for the linear machine. These dynamic models are then utilized for synthesis of the two sliding mode control laws for flux regulation and combined speed and thrust force control. The sliding mode control laws produce the orthogonal components of command voltage in the stator flux reference frame which are then applied to the machine by a space vector pulsewidth modulated inverter. Importantly, integral action is also directly included in the control laws by using a modified first-order plus integral sliding condition. The integral action eliminates the steady-state error and provides additional restoring effort in the stator flux and speed tracking combined with thrust force control. Lyapunov stability analysis proves the global asymptotic stability of the proposed control scheme. The effectiveness of the proposed method is validated by extensive experimentation on a prototype linear machine. Practical results demonstrate excellent transient and steady-state speed control performance of the proposed scheme when compared to the state-of-the-art methods.**

***Index Terms*—Direct thrust force control (DTFC), linear permanent magnet synchronous motor (linear PMSM), sliding mode control.**

I. Introduction

DIRECT TORQUE CONTROL (DTC) for induction motors (IMs) and rotational permanent magnet synchronous motors (PMSMs) [1]–[4] and direct thrust force control (DTFC) for linear PMSMs [5]–[9] have become widespread control

Manuscript received December 4, 2017; revised March 2, 2018; accepted May 3, 2018. Date of publication May 20, 2018; date of current version February 5, 2019Recommended for publication by Associate Editor J. E. Ojo. *(Corresponding author: Muhammad Ali Masood Cheema.)*

M. A. M. Cheema is with the Northern Transformer Corporation, Maple, ON L6A 4P5, Canada (e-mail:

pling time into three intervals during which two adjacent active vectors and a zero-voltage vector are applied to the machine to generate any arbitrary command voltage. The hysteresis controllers of [12]–[14] for dq axes voltages can only take discrete values $-V_{\rm dc}$ or $V_{\rm dc}$, with $V_{\rm dc}$ being the dc-link voltage of the VSI. It should be noted that a valid dq axes to stationary $\alpha\beta$ axes transformation cannot be performed for these voltage values [15]. Therefore, the control schemes of [12]–[14] cannot be used in conjunction with the SV-PWM technique to reduce ripple in torque/thrust force [15]–[17].

A variable-structure-based direct torque control with SV-PWM is reported in [18] for rotational PMSMs. It demonstrates the excellent transient torque control with reduced steady-state ripple. However, a separate PI controller is used for speed control and consequently speed dynamics are compromised.

The studies in [19]–[22] report a sliding mode controller for the rotational PMSM which combines the speed and q-axis current control (based on the vector control principle) in one controller. It is important to note that the sliding mode control methods of [19]–[22] do not consider the stator flux and torque (thrust force in case of linear PMSM) as system state variables, and therefore, transient response may become slow.

Application of sliding mode control law in conjunction with SV-PWM to achieve combined speed and direct thrust force control with reduced force ripple requires the sliding mode control law to be formulated in terms of the thrust force and mover's speed as state variables. There is, so far, no literature regarding the application of SV-PWM based sliding mode control to the linear-PMSM (or PMSM) for combined speed and direct thrust force control (or direct torque control). The key contribution of this research is to formulate an SV-PWM based sliding mode control law for combined speed and direct thrust force control of the linear PMSMs. For this purpose, a nonlinear second-order state-space model of the linear PMSM in a synchronously rotating stator flux vector xy-reference frame for combined dynamics of speed and thrust force as system states is used to formulate the sliding mode control law for combined control of speed and thrust force. The sliding mode control law for stator flux regulation is formulated based on the first-order linear stator flux dynamics. Moreover, an integral action is also directly included in the control laws by using a modified first-order plus integral sliding condition [23], [24]. The integral action eliminates the steady-state error and provides additional restoring effort in the stator flux and speed tracking combined with direct thrust force control. Experimental results from a prototype surface-mount linear PMSM demonstrate the improvement in terms of steady state and transient speed, thrust force, and stator flux responses of the proposed approach under various operating conditions when compared to the prior techniques of [25] and [26].

The dynamic model for the linear PMSM, comprising linear stator flux dynamics and second-order nonlinear combined speed and thrust force dynamics, expressed in synchronously rotating stator flux vector reference frame, is detailed in Section II. Section III provides the brief details of the state-of-the-art techniques of [25] and [26]. The description of the sliding mode control and its application to the linear PMSM for combined speed and direct thrust control is given in Sections IV and V, respectively. Experimental results and conclusions are provided in Sections V and VI, respectively.

II. Dynamic Model of the Linear PMSM in the Synchronously Rotating Reference Frame

The dynamic model of the surface-mount linear PMSM in the synchronously rotating stator flux vector based xy-reference frame can be expressed as [26], [27]

$$v_x = R_s i_x + \frac{d\lambda_s}{dt} \tag{1}$$

$$v_y = R_s i_y + \omega_s \lambda_s = R_s i_y + \underbrace{\left(P\frac{\pi}{\tau} v_m + \frac{d\delta}{dt} \right)}_{\omega_s} \lambda_s \tag{2}$$

where v_x, v_y, i_x, i_y are the x-axis and y-axis components of the stator voltage space vector and stator current space vector, respectively, and R_s is the stator resistance in ohms. λ_s and ω_s are the magnitude and angular speed (synchronous speed) of the stator flux vector in Wb and elec. rad/s, respectively. δ is the angle between stator flux space vector and mover's permanent magnet flux space vector called as load angle is expressed in elect. rad, and v_m is the mover speed in m/s. P and τ are the number of pole pairs and the pole pitch in meters, respectively. The electromagnetic thrust force F_T of a surface-mount linear PMSM is given as [22]

$$F_T = P k_F \frac{3}{2} \frac{\pi}{\tau L_s} \lambda_s \lambda_f \sin\delta \tag{3}$$

where λ_f is the permanent magnet flux (Wb) and L_s is the machine inductance (H). k_F is a constant which is used to quantify the end effects in the linear PMSM. The electromagnetic thrust force F_T for an interior permanent magnet (IPM) linear PMSM is given as [23]

$$F_T = P k_F \frac{3\pi\lambda_s}{4\tau L_d L_q} \left[2\lambda_f L_q \sin\delta - \lambda_s \left(L_d - L_q \right) \sin 2\delta \right]. \tag{4}$$

In (4), L_d and L_q are the d-axis and q-axis inductances (H), respectively, for the IPM linear PMSM.

A. Stator Flux Dynamics

The dynamics of the stator flux regulation are from (1)

$$\frac{d\lambda_s}{dt} = v_x - R_s i_x. \tag{5}$$

According to (5), the stator flux can be controlled by v_x and the resistive drop $R_s i_x$ is assumed as a disturbance.

B. Combined Speed and Thrust Force Nonlinear Dynamics

Equations (3) and (4) can be linearized using Taylor's series expansion at load angle δ_0 as [26]–[29]

$$F_T = K\left(\delta - \delta_0\right) + F_0 \tag{6}$$

where $K = dF_T(\delta)/d\delta|_{\delta=\delta_0}$, and $F_0 = F_T(\delta_0)$.

TABLE I
EXPERIMENTAL LINEAR PMSM PROTOTYPE PARAMETERS

Pole Pairs	3
Max. Current (A)	3.27
λ_f PM Flux (mWb)	84.6
L_s (mH)	1.95
R_s (ohms)	3.01
τ (m)	0.0256
M (kg)	1.25
B (friction constant)	0.14
Rated Cont. Force (N)	52
Max Peak Force (N)	312

In (6), K is a linearization coefficient and is a function of thrust force F_T [27], [29]. For a linear PMSM, it is evaluated at $\delta_0 = 0$ leading to $F_0 = 0$ [27]. It is important to note that (6) is valid for both surface-mounted and IPM linear PMSMs. In this paper, for a surface-mount linear PMSM (6) will be achieved by linearizing (3) using the parameters of the prototype linear PMSM of Table I. For a surface-mount linear PMSM, the value of the linearization coefficient K can be expressed in terms of thrust force F_T as [27]

$$K\left(F_T\right) = Pk_F \frac{3}{2}\frac{\pi}{\tau L_s}\lambda_{\mathrm{ref}}\lambda_f \sqrt{1-\left(\frac{2\tau L_s}{3\pi P k_F \lambda_{\mathrm{ref}}\lambda_f}F_T\right)^2}. \tag{7}$$

From (7) and parameters of the prototype linear PMSM, as the thrust force varies from 0 to the peak value of 312 N, the variation in magnitude K is less than 1.2% and K remains almost constant [27]. The stator flux reference λ_{ref} is selected according to maximum force per ampere (MFPA) and is given as [26], [27]

$$\lambda_{\mathrm{ref}}\left(F_T\right) = \sqrt{\lambda_f^2 + \left(\frac{2}{3}\frac{\tau L_s}{\pi P k_F}F_T\right)^2}. \tag{8}$$

For the prototype linear PMSM, as given in Table I, λ_{ref} is set to 0.0846 Wb in the prototype system [27]. The mechanical dynamics of the linear PMSM can be given as [26]

$$\frac{dv_m}{dt} = \frac{1}{M}F_T - \frac{B}{M}v_m - \frac{1}{M}F_L \tag{9}$$

where M is the mover's mass in Kg, B is the friction constant in Kg·m/s, and F_L is the load force in N.

The mechanical dynamics of the linear PMSM can be combined with (2), (6), (7), and (9) as detailed in [26] to result in the nonlinear combined dynamics of speed and thrust force as

$$\dot{X} = F\left(X\right) + G\left(X\right)u + D\left(t\right) \tag{10}$$

where $\xi = \frac{3\pi P\lambda_{\mathrm{ref}}(F_T)}{2\tau R_s}$, $X = \left[\begin{smallmatrix} x_1 \\ x_2 \end{smallmatrix}\right] = \left[\begin{smallmatrix} F_T \\ v_m \end{smallmatrix}\right]$

$$F\left(X\right) = \begin{bmatrix} f_1\left(x_1, x_2\right) \\ f_2\left(x_1, x_2\right) \end{bmatrix} = \begin{bmatrix} \dfrac{-K\left(F_T\right)}{\xi\lambda_{\mathrm{ref}}\left(F_T\right)}F_T - \dfrac{K\left(F_T\right)P\pi}{\tau}v_m \\ \dfrac{1}{M}F_T - \dfrac{B}{M}v_m \end{bmatrix},$$

$$G\left(X\right) = \begin{bmatrix} b\left(F_T\right) \\ 0 \end{bmatrix} = \begin{bmatrix} \dfrac{K\left(F_T\right)}{\lambda_{\mathrm{ref}}\left(F_T\right)} \\ 0 \end{bmatrix}, u = v_y,$$

$$D\left(t\right) = \begin{bmatrix} 0 \\ -\dfrac{1}{M} \end{bmatrix} F_L.$$

The combined speed and thrust force dynamics for the linear PMSM expressed in (10) represent a second-order nonlinear single-input single-output (SISO) system such that the y-axis voltage v_y is the only control input. Therefore, only one state variable can be tracked. Considering the speed control as the main control objective, v_m is a natural choice for state tracking. The dynamic (10) clearly indicates that control of the thrust force F_T is implicitly combined with that of v_m. It can be assumed with sufficient rationality that all states can be either estimated or measured, therefore, v_m can be expressed as the tracking output y in state-space form as

$$y = v_m = \begin{bmatrix} 0 & 1 \end{bmatrix}\begin{bmatrix} F_T \\ v_m \end{bmatrix} = H\left(X\right). \tag{10-a}$$

The schematic illustration of the combined speed and thrust dynamics according to (10) and (10a) is shown in Fig. 1.

The dynamic model of (10) and (10a) is generally valid for all types of linear PMSMs in the sense that it is based on the generalized characteristics of K and λ_{ref} and does not restrict these quantities to be constant. Due to variation or uncertainty in the machine parameters caused by atmospheric factors or measurement errors is bounded [30], [31], therefore, estimation errors Δf_1 and Δf_2 in $f_1(x_1, x_2)$ and $f_2(x_1, x_2)$ are bounded by some know functions $F_1(x_1, x_2)$ and $F_2(x_1, x_2)$, respectively [30]–[33]

$$\Delta f_1 \le F_1\left(x_1, x_2\right) \tag{11}$$

$$\Delta f_2 \le F_2\left(x_1, x_2\right). \tag{12}$$

In (10), the control gain $b(F_T)$ of the control input v_y has also known bounds [30]

$$0 < b_{\min} \le b\left(F_T\right) \le b_{\max}. \tag{13}$$

The estimated value of $\hat{b}(F_T)$ of gain $b(F_T)$ can be expressed as [30]–[33]

$$\hat{b}\left(F_T\right) = \sqrt{b_{\min}b_{\max}}. \tag{14}$$

The above equation can also be expressed as [30]

$$\zeta^{-1} \le \frac{\hat{b}\left(F_T\right)}{b\left(F_T\right)} \le \zeta \tag{15}$$

where $\zeta = \sqrt{\frac{b_{\max}}{b_{\min}}}$.

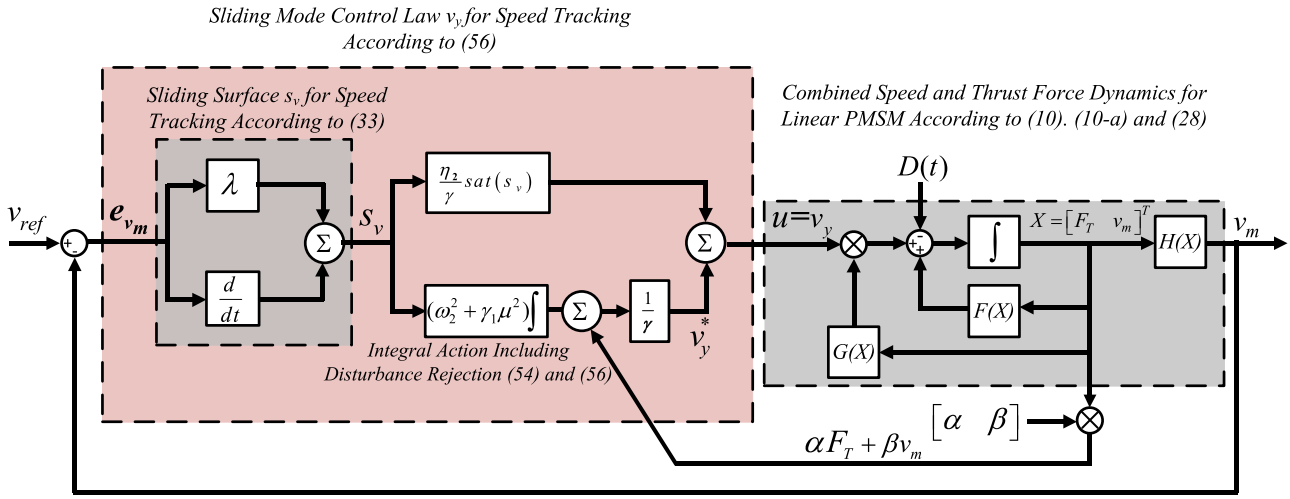

Fig. 1. Schematics describing the sliding mode control with first-order plus integral sliding condition for nonlinear combined speed and thrust force dynamics and the proposed of (10) and (10a).

It is clear that (10) is a second-order nonlinear differential equation with the mover's speed v_m and the thrust force F_T as system states and y-axis voltage v_y as the control input. It is important to note that for constant values of K and $\lambda_{\rm ref}$, as in the case of prototype under study, (10) becomes a second-order linear differential equation. The differential (10) provides the basis to formulate the sliding mode control law in terms of the stator thrust force and mover's speed as system state and to achieve combined control of the thrust force and the mover's speed, as explained in Section IV. The dynamic model (10) does not inherit integral action, therefore, to eliminate the steady-state error, the integral action must be provided by the control law. The sliding mode control for stator flux regulation is formulated using (5) such that stator flux λ_s tracks the reference flux value $\lambda_{\rm ref}$ as determined by (8) under the MFPA trajectory.

III. State-of-the-Art SV-PWM Based DTFC Techniques

In this paper, two recently proposed SV-PWM based DTFC schemes [25], [26] for the linear PMSM are benchmarked as state-of-the-art techniques. In [25], a PI controller based DTFC scheme incorporating SV-PWM is detailed. The research in [26] proposes a linear quadratic regulator (LQR) based combined speed and direct thrust force control scheme utilizing SV-PWM for a linear PMSM. These states-of-the-art techniques will be described briefly in the following.

A. PI-Based DTFC

An SV-PWM based DTFC scheme for the linear PMSM [25] (referred to as "PI-DTFC") is based on the concept of decoupled control of the thrust force and the stator flux. In this scheme, the stator flux and thrust force are controlled by two PI controllers and the speed is regulated by a third PI controller.

B. LQR-Based Combined Speed and DTFC

In [26], an SV-PWM based optimal control scheme (referred to as optimal DTFC), for combined speed and direct thrust force control of PMSM is proposed. A multiple-input multiple-output state-space model having stator flux, thrust force and mover's speed as states is formulated for the linear PMSM. This model is then used to formulate an optimal linear state feedback law for combined speed and direct thrust force control based on the LQR approach. The linear state feedback law to generate control voltages v_x and v_y is [26]

$$\begin{bmatrix} v_x \\ v_y \end{bmatrix} = -\begin{bmatrix} k_\lambda & 0 & 0 & -k_{i\lambda} & 0 \\ 0 & k_F & k_v & 0 & -k_{iv} \end{bmatrix} \begin{bmatrix} \lambda_s \\ F_T \\ v_m \\ \xi_s \\ \xi_v \end{bmatrix} \tag{16}$$

where $\xi_s = \int(\lambda_{\rm ref} - \lambda_s)dt, \xi_v = \int(v_{\rm ref} - v_m)dt$, and $v_{\rm ref}$ is the reference speed. In (16), $k_\lambda, k_{i\lambda}, k_F, k_v$, and k_{iv} are the controller gains and determined using LQR-based approach, as detailed in [26].

IV. Sliding Mode Control

Sliding mode control is a nonlinear control architecture that can tolerate parameter variation and imprecision in the plant model [8], [9]. Slotine [31]–[33] further advanced the concept of sliding mode control by formulation of the tracking control of the general SISO nonlinear system described as

$$\dot{x}_i = x_{i+1}, i = 1, \ldots, n-1 \text{ and } x_1 = x \tag{17}$$

$$\dot{x}_n = f(X;t) + g(X;t)\,u + d(t) \tag{18}$$

where $X = [x,\ \dot{x}, \ldots,\ x^{n-1}]^T$ is the state vector.

In (18), u is the control input. The function $f(X;t)$ (generally nonlinear) is not exactly known, however, the imperfection Δf in the estimated value $\hat{f}(X;t)$ is bounded by a known continuous function $F_b(X;t)$. Similarly, the control gain $g(X;t)$ is not precisely known but is of constant sign and the imperfection Δg in estimated value $\hat{g}(X;t)$ is bounded by a continuous function

$G_b(X;t)$ and the disturbance $d(t)$ is also bounded. The control problem is that the state vector X should track the reference state vector X_d with satisfactory tracking precision. The desired state vector X_d is given as

$$X_d = \left[x_d,\ \dot{x}_d, \ldots,\ x_d^{n-1}\right]^T. \tag{19}$$

The tracking error vector between the desired state vector X_d and the actual state vector X is $\tilde{X}$ and is

$$\tilde{X} : X_d - X = \left[\tilde{x},\ \dot{\tilde{x}}, \ldots,\ \tilde{x}^{n-1}\right]^T. \tag{20}$$

The time varying sliding surface to achieve the tracking is formulated in terms of the tracking error $\tilde{x}$ and is given as [31]–[33]

$$s_c(X;t) = \left(\frac{d}{dt} + \lambda\right)^{n-1} \tilde{x}dt \tag{21}$$

where n is the order of the system and λ is a positive constant. A first-order system has $n = 1$.

The control law u to achieve the tracking is given as [8]

$$u = u_{\mathrm{eq}}(X;t) + \rho_0 \mathrm{sgn}(s_c). \tag{22}$$

In (22), the concept of equivalent control $u_{\mathrm{eq}}(X;t)$ is also attributed to Utkin [9]–[15]. $u_{\mathrm{eq}}(X;t)$ is a state feedback law which computed by solving $\dot{s} = 0$ for u and assuming Δf and Δg to be zero. ρ_0 is a constant gain and sgn is the signum function defined as [9], [31]–[33]

$$\mathrm{sgn}(s_c) = \begin{cases} 1 & \text{if } s_c > 0 \\ -1 & \text{if } s_c < 0. \end{cases} \tag{23}$$

According to Slotine, u is selected to satisfy the η-reachability condition (so-called sliding condition) given as [8], [31]–[33]

$$\frac{1}{2}\frac{d}{dt}s_c^2(X;t) \le \eta |s_c(X;t)| \tag{24}$$

where η is a positive constant.

An integral sliding surface formulated in terms of the integral of the tracking error is [21], [33]

$$s_c(X;t) = \left(\frac{d}{dt} + \lambda\right)^n \int \tilde{x}dt. \tag{25}$$

It is important to note that (25) does not add the integral action directly in the equivalent control law $u_{\mathrm{eq}}(X;t)$. However, it can be observed from (22) that the sliding surface s_c containing the integral term appears inside the discontinuous $\mathrm{sgn}(\cdot)$ function in the control law and, therefore, continuous pure integrator action is not available directly which leads to a steady-state error. Special steps are required to include a pure integrator action in the equivalent control law $u_{\mathrm{eq}}(X;t)$ to ensure a zero steady-state error.

A. Sliding Mode Control With Augmented Integral Action

The dynamic system of (17) and (18) can be further generalized by considering the fact that all the state derivatives can be expressed as nonlinear functions of two or more states instead of only one state, therefore, (17) and (18) become

$$\dot{x}_i = f_i(X;t), i = 1, \ldots n-1 \tag{26}$$

$$\dot{x}_n = f_n(X;t) + g(X;t)u + d(t). \tag{27}$$

The compact form of (26) and (27) is given as

$$\dot{X} = F(X) + G(X)u + D(t) \tag{28}$$

where

$$F(X) = \begin{bmatrix} f_1(X;t) \\ f_2(X;t) \\ \vdots \\ f_n(X;t) \end{bmatrix}, G(X) = \begin{bmatrix} 0 \\ 0 \\ \vdots \\ g(X;t) \end{bmatrix}, \text{and}$$

$$D(t) = \begin{bmatrix} 0 \\ 0 \\ \vdots \\ d(t) \end{bmatrix}.$$

It is important to note that (28) can be validly used to describe the dynamic model given in (10) of the prototype linear PMSM. The sliding manifold $s_c(X;t)$ for the dynamics of (28) is a function of the tracking error and is given by (21).

In order to modify the η-reachability condition so that the pure integral action can be augmented in the control law, the following Lyapunov candidate function is defined [23], [24]:

$$V = \frac{1}{2}s_c^2 + \frac{1}{2}\omega_n^2\left(\int_0^t s_c dt\right)^2. \tag{29}$$

By applying the Lyapunov stability criterion for stability $\dot{V} \le 0$, the sliding condition is obtained as

$$s_c.\left(\dot{s}_c + \omega_n^2 \int_0^t s_c dt\right) \le 0. \tag{30}$$

In other words $\dot{s}_c + \omega_n^2 \int_0^t s_c dt \ge 0$, when $s_c < 0$ and $\dot{s}_c + \omega_n^2 \int_0^t s_c dt < 0$, when $s_c \ge 0$

Now the modified η-reachability condition can be expressed as

$$s_c\left(\dot{s}_c + \omega_n^2 \int_0^t s_c dt\right) \le \eta |s_c|. \tag{31}$$

The equivalent control law $u_{\mathrm{eq}}(X;t)$ is now evaluated by solving $\dot{s}_c + \omega_n^2 \int_0^t s_c dt = 0$ for the control input u [24]. In (29), ω_n is called as the equivalent spring constant [24], the integral of the sliding surface s_c in (29) provides an additional restoring effort and the dynamic behavior of the effect of the integral action can be tuned by ω_n. It is important to note that the modified η-reachability condition adds an integral action directly into the equivalent control law $u_{\mathrm{eq}}(X;t)$. The damping of the system response is controlled by η and a higher value of η results in less oscillation in the system response, whereas a low value of η causes a lightly damped oscillation in the system response such that the frequency of the oscillation is determined

by ω_n [23], [24]. A detailed tuning mechanism for η and ω_n is reported in [24].

V. Proposed Combined Speed and Direct Thrust Force Control of the Linear PMSM Based on Integral Sliding Mode Control

A. Sliding Surface for the Stator Flux Regulation

The sliding surface s_λ for the stator flux regulation dynamics of (5) can be given from (21) for $n = 1$ as

$$s_\lambda = e_\lambda \tag{32}$$

where $e_\lambda = \lambda_{\rm ref} - \lambda_s$ is the flux tracking error.

B. Sliding Surface for Speed Regulation

The sliding surface s_v for the combined speed and thrust force dynamics of (10) is computed from (21) for $n = 2$ as

$$s_v = \frac{de_{v_m}(t)}{dt} + \lambda_1 e_{v_m}(t) \tag{33}$$

where $e_{v_m} = v_{\rm ref} - v_m$ is the speed tracking error, $v_{\rm ref}$ is the reference speed, and λ_1 is a strictly positive constant.

C. Control Law for Stator Flux Regulation

Differentiating (32)

$$\dot{s}_\lambda = \left(\dot{\lambda}_{\rm ref} - \dot{\lambda}_s\right). \tag{34}$$

Since, $\dot{\lambda}_{\rm ref} = 0$, and from (5), (34) becomes

$$\dot{s}_\lambda = R_s i_x - v_x. \tag{35}$$

The control law for the stator flux to ensure the condition $\dot{s}_\lambda + \omega_1^2 \int_0^t s_\lambda dt = 0$ is

$$v_x = v_x^* - \eta_1 \mathrm{sgn}\,(s_\lambda) \tag{36}$$

where η_1 is a positive constant, and

$$v_x^* = -R_s i_x - \omega_1^2 \int_0^t s_\lambda dt. \tag{37}$$

The control law (36) satisfies the sliding condition for global stability [24]

$$s_\lambda \left(\dot{s}_\lambda + \omega_1^2 \int_0^t s_\lambda dt\right) \le \eta_1 |s_\lambda|. \tag{38}$$

D. Control Law for Combined Speed and Thrust Force Regulation

Taking the time derivative of (33)

$$\dot{s}_v = (\ddot{v}_{\rm ref} - \ddot{v}_m) + \lambda_2 (\dot{v}_{\rm ref} - \dot{v}_m). \tag{39}$$

The value of $\ddot{v}_m$ can be obtained from (9) as

$$\ddot{v}_m = \frac{1}{M}\dot{F}_T - \frac{B}{M}\dot{v}_m - \frac{1}{M}\dot{F}_L. \tag{40}$$

In general, the load force F_L is constant during steady state and does not change abruptly, therefore, $\dot{F}_L = 0$, [34], [35], (40) becomes

$$\ddot{v}_m = \frac{1}{M}\dot{F}_T - \frac{B}{M}\dot{v}_m. \tag{41}$$

Substituting the value of $\dot{F}_T$ and $\dot{v}_m$ from (10) into (41)

$$\ddot{v}_m = \frac{1}{M}\left(\frac{-K}{\xi\lambda_{\rm ref}}F_T - KP\frac{\pi}{\tau}v_m + \frac{K}{\lambda_{\rm ref}}v_y\right) - \frac{B}{M}\left(\frac{1}{M}F_T - \frac{B}{M}v_m - \frac{1}{M}F_L\right). \tag{42}$$

The reference speed $v_{\rm ref}$ is a constant during steady state and, therefore

$$\ddot{v}_{\rm ref} = \dot{v}_{\rm ref} = 0. \tag{43}$$

Substituting (43) and the value of $\dot{v}_m$ and $\ddot{v}_m$ from (9) and (42), respectively, into (39) and rearranging

$$\dot{s}_v = \alpha F_T + \beta v_m + \mu F_L - \gamma v_y \tag{44}$$

where, $\alpha = (\frac{K}{M\xi\lambda_{\rm ref}} + \frac{B}{M^2} - \frac{\lambda_2}{M})$, $\beta = (KP\frac{\pi}{M\tau} + \frac{B^2}{M^2} + \lambda_2\frac{B}{M})$, $\mu = (\frac{\lambda_2}{M} - \frac{B}{M^2})$, and $\gamma = \frac{K}{M\lambda_{\rm ref}}$.

The equivalent control law v_y^* to achieve the condition $\dot{s}_v + \omega_2^2 \int_0^t s_v dt = 0$ is defined from [24]

$$v_y^* = \frac{1}{\gamma}\left(\alpha F_T + \beta v_m + \omega_2^2 \int_0^t s_v dt + \mu\hat{F}_L\right). \tag{45}$$

Since the load force F_L is usually an unknown quantity, therefore, in (45), the estimated value of load force $\hat{F}_L$ is used.

In order to achieve the sliding mode condition, the discontinuous control $\mathrm{sgn}\,(s_v)$ is included in the equivalent control law of (45) as [24], [31]–[33]

$$v_y = v_y^* + \frac{\eta_2}{\gamma}\mathrm{sgn}\,(s_v) \tag{46}$$

where γ and η_2 are the strictly positive constants.

In order to rationalize and establish the stability of the controller of (46), the following Lyapunov candidate function [24], [31] is defined:

$$V = \frac{1}{2}s_v^2 + \frac{1}{2}\omega_2^2\left(\int_0^t s_v dt\right)^2 + \frac{1}{2\gamma_1}\tilde{F}_L^2 \tag{47}$$

where $\tilde{F}_L = F_L - \hat{F}_L, \gamma_1 > 0$, and differentiating (47)

$$\dot{V} = s_v\left(\dot{s}_v + \omega_2^2\int_0^t s_v dt\right) - \frac{1}{\gamma_1}\dot{\hat{F}}_L\tilde{F}_L. \tag{48}$$

Substituting (44) into (48)

$$\dot{V} = s_v\left(\alpha F_T + \beta v_m + \mu F_L - \gamma v_y + \omega_2^2\int_0^t s_v dt\right) - \frac{1}{\gamma_1}\dot{\hat{F}}_L\tilde{F}_L. \tag{49}$$

Substituting (45) and (46) into (49), and simplifying

$$\dot{V} = s_v\left(-\eta_2\mathrm{sgn}\,(s_v) + \mu\tilde{F}_L\right) - \frac{1}{\gamma_1}\dot{\hat{F}}_L\tilde{F}_L. \tag{50}$$

Since, $s_v \times \text{sgn}(s_v) = |s_v|$, therefore, (50) becomes

$$\dot{V} = \left(-\eta_2 |s_v| + \tilde{F}_L \left(\mu s_v - \frac{1}{\gamma_1}\dot{\hat{F}}_L\right)\right). \tag{51}$$

To ensure the global stability of the controller, $\dot{V} < 0$ suggests the following expression to estimate the load force $\hat{F}_L$:

$$\hat{F}_L = \gamma_1 \mu \int_0^t s_v dt. \tag{52}$$

Hence, (51) reduces to

$$\dot{V} = -\eta_2 |s_v| < 0. \tag{53}$$

Since, η_2 is a positive constant, therefore, $\dot{V}$ is strictly negative when the load force is estimated using (52). Now the substitution of (52) into (51) results

$$v_y^* = \frac{1}{\gamma}\left(\alpha F_T + \beta v_m + \omega_2^2 \int_0^t s_v dt + \underbrace{\gamma_1 \mu^2 \int_0^t s_v dt}_{\substack{\text{disturbance} \\ \text{rejection}}}\right). \tag{54}$$

In (54), ω_2 determines the natural frequency of the damped oscillations in the speed response and can be used to tune the integral action [24]. It is important to note that the underlined term in (54) is the estimated load force according to (52) and acts as disturbance rejection which cancels out the effect of load disturbance in dynamic model given by (10). The two integral terms in (54) can be combined into a single term that provides the integral action as wells as disturbance rejection at the same time, rearranging terms in (54) results

$$v_y^* = \frac{1}{\gamma}\left(\alpha F_T + \beta v_m + \left(\omega_2^2 + \gamma_1 \mu^2\right) \int_0^t s_v dt\right). \tag{55}$$

From (46) and (55), the control law v_y is expressed as

$$v_y = \frac{1}{\gamma}\left(\alpha F_T + \beta v_m + \left(\omega_2^2 + \gamma_1 \mu^2\right) \int_0^t s_v dt + \eta_2 \text{sgn}(s_v)\right). \tag{56}$$

E. Chattering Reduction

It is important to note that "sgn" function in the control laws of (36) and (46) introduces the chattering, which can be reduced by introducing a boundary layer of thickness ε around the sliding manifold $s_c(x;t) = 0$. This is achieved by replacing the "sgn" function with "sat" function defined as [31]–[33]

$$\text{sat}(s_c) = \begin{cases} 1 & \text{if } s_c > \varepsilon \\ \dfrac{s_c}{\varepsilon} & \text{if } |s_c| \le \varepsilon \\ -1 & \text{if } s_c < -\varepsilon. \end{cases} \tag{57}$$

VI. Experimental Results

The proposed sliding mode control scheme for combined speed and DTFC (referred to as SM-DTFC) has been practically validated on the prototype surface-mount linear PMSM control system. The main hardware components of the experimental setup are illustrated in Fig. 2. The parameters of the surface-mount linear PMSM are provided in Table I. Experimental results indicate the improved performance of the SM-DTFC method in terms of steady-state error and transient response of the stator flux, thrust force and speed when compared with the prior PI-DTFC [25] and optimal DTFC [26] methods.

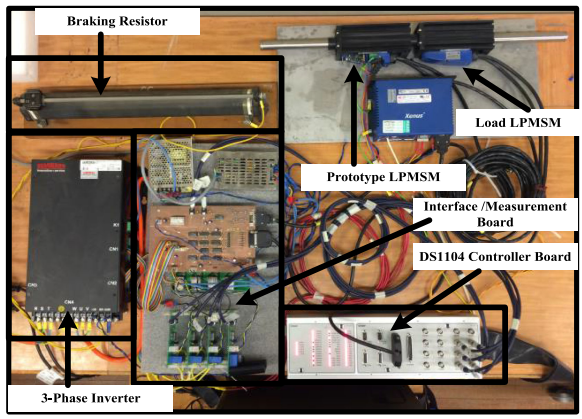

Fig. 2. Experimental setup showing the prototype linear PMSM, voltage source inverter, and the control circuitry.

The proposed SM-DTFC is digitally implemented according to the block diagram of Fig. 3 using a dSPACE DS-1104 controller. The sample time is chosen to be 200 μs. Moreover, PI-DTFC and Optimal-DTFC are also implemented digitally with the same sample time as detailed in [25] and [26]. The integrators used in both the Optimal-DTFC and PI-DTFC have an antiwindup scheme with the antiwindup gains for all the integrators set at unity. The controller gains for PI-DTFC and Optimal-DTFC are same as detailed in [26].

A. Startup Response

The startup speed responses of the surface-mount linear PMSM under the PI-DTFC, Optimal-DTFC, and the SM-DTFC are compared. The speed, flux, thrust force, and stator currents for the Optimal-DTFC and the SM-DTFC during the startup transient are shown in Fig. 4(a)–(c) respectively.

It is clear from Fig. 4(a) that during the startup transient under PI-DTFC, the speed response exhibits a speed dip immediately after reaching the speed reference of 200 mm/s. However, under SM-DTFC, the speed dip is noticeably reduced.

Fig. 4 clearly shows that the thrust force under SM-DTFC settles to steady-state faster compared to PI-DTFC and Optimal-DTFC. The magnified views of the startup speed response for both PI-DTFC and the SM-DTFC are shown in Fig. 5(a) and (b), respectively. It is clear from Fig. 5(a) and (c) that the speed response under the SM-DTFC is 15% faster compared to that of PI-DTFC. It is also observed from Fig. 5(b) and (c) that SM-DTFC has also a faster transient response compared to the Optimal-DTFC.

In addition, for quantitative analysis, the integral of absolute error (IAE) indices for the speed error plots for PI-DTFC,

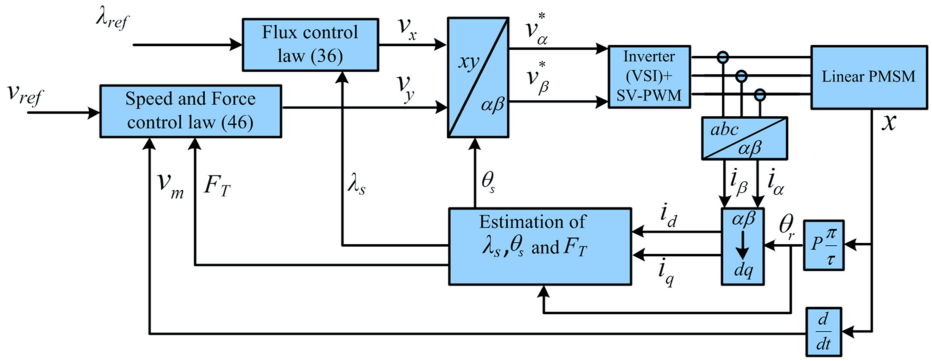

Fig. 3. Proposed sliding mode based combined speed and thrust control of linear PMSM (SM-DTFC), the integral action is added by modification of the reachability condition.

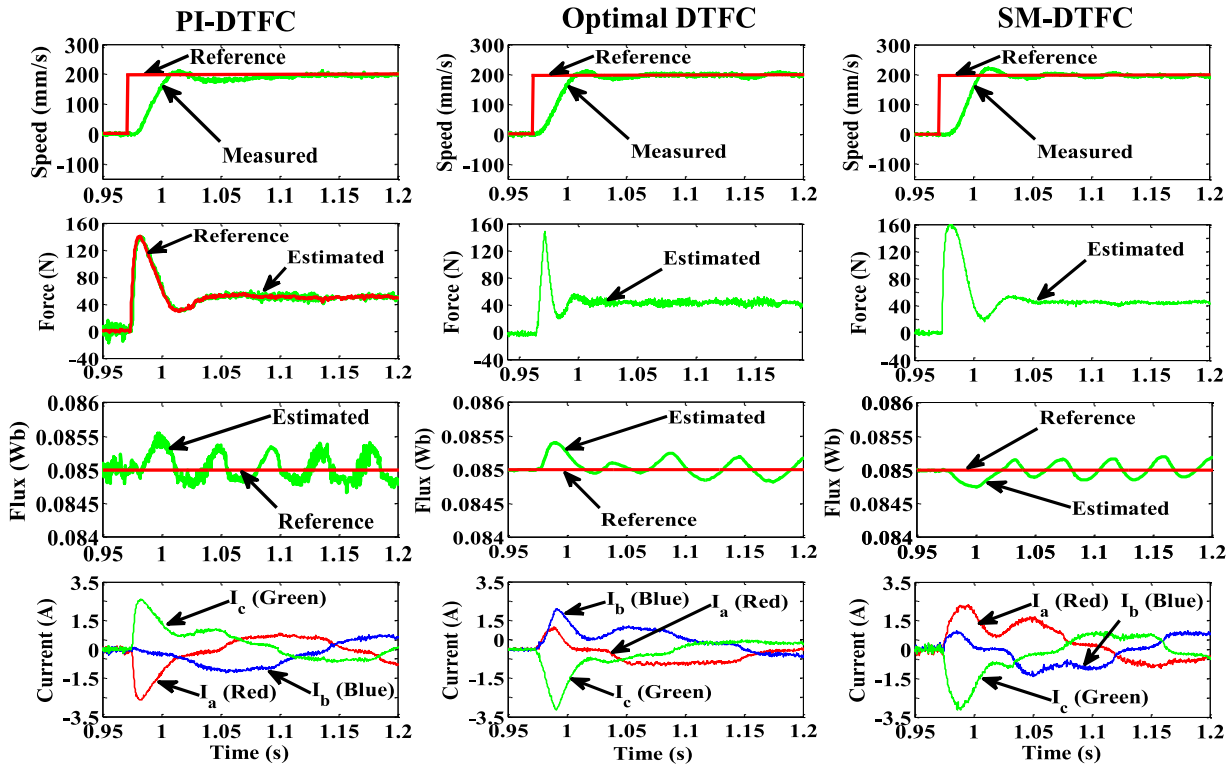

Fig. 4. Startup performance from 0 to 200 mm/s. Speed, thrust force, stator flux, and stator phase currents responses are shown from top to bottom, respectively. (a) For PI-DTFC. (b) For Optimal-DTFC. (c) For SM-DTFC (experiment).

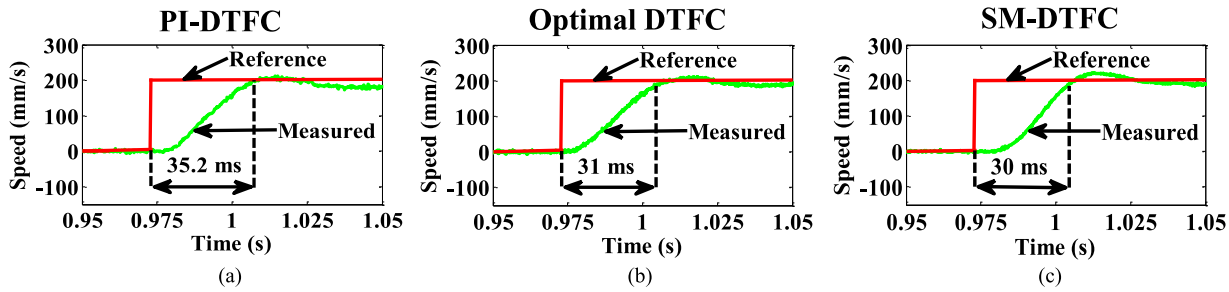

Fig. 5. Magnified view of the speed response during startup. (a) PI-DTFC. (b) Optimal-DTFC. (c) SM-DTFC (experiment).

TABLE II
COMPARISON OF TRANSIENT PERFORMANCE OF PI-DTFC, OPTIMAL-DTFC, AND THE SM-DTFC USING IAE INDEX

Type of transient phenomena	IAE Index for Speed error		
	PI-DTFC	Optimal-DTFC	SM-DTFC
Start-up (0 to 200mm/s)	23721	19619	18975
Speed reversal (-600 to 600 mm/s)	210430	189370	188775

TABLE III
COMPARISON OF STEADY-STATE PERFORMANCE OF PI-DTFC, OPTIMAL-DTFC, AND SM-DTFC

600 mm/s, 52 N	PI-DTFC	Optimal-DTFC	SM-DTFC
λ_{rip} (%)	0.34	0.21	0.19
F_{rip} (%)	10.48	5.83	5.79
v_{rip} (%)	1.92	1.11	1.08

Optimal-DTFC, and SM-DTFC during the startup are computed, as shown in Table II. The IAE index for the speed error plot under the SM-DTFC is reduced by 20% compared to that of the PI-DTFC.

It is observed from Table II that the IAE index of SM-DTFC is also reduced compared to the Optimal-DTFC.

The magnified views of the thrust force response during startup for the PI-DTFC, Optimal-DTFC, and SM-DTFC are shown in Fig. 6. It is evident from Figs. 5 and 6 that when the speed command steps from 0 to 200 mm/s at 0.975 s, the corresponding thrust force under the SM-DTFC reaches a peak value of 160 N, whereas the thrust force under the PI-DTFC peaks at 139 N, the additional force produced results in the faster speed response for the SM-DTFC. Moreover, it is also evident from Fig. 6 that the thrust force under the SM-DTFC settles to steady state 4.4 ms faster than that of PI-DTFC. It can be concluded from these experimental results that the combined control of the speed and thrust force achieved under the SM-DTFC can deliver faster speed response during startup compared to the PI-DTFC. Similar conclusions can be drawn from the comparison of Fig. 6 for Optimal-DTFC and SM-DTFC, respectively.

The stator flux responses for the PI-DTFC, Optimal-DTFC, and SM-DTFC are shown in Fig. 4(a)–(c), respectively. It is clear from Fig. 4 that under SM-DTFC, the average steady-state ripple in the stator flux response after settling to steady state is minimum compared to the PI-DTFC and Optimal-DTFC.

B. Speed Reversal and Steady-State Response

The speed reversal and steady-state performance of the linear PMSM under the PI-DTFC, Optimal-DTFC, and SM-DTFC are compared. The speed, stator flux, thrust force, and stator currents for the PI-DTFC, Optimal-DTFC, and the SM-DTFC during the speed reversal transient from –600 mm/s to 600 mm/s and steady state at 600 mm/s are shown in Fig. 7(a)–(c), respectively. Fig. 7(a) illustrates that the oscillation in speed response after the speed is reversed from –600 mm/s and reaches 600 mm/s is reduced under the SM-DTFC compared to PI-DTFC. It is observed from Fig. 7(b) and (c) that the overshoot in the speed response after the speed is reversed from –600 mm/s and reaches 600 mm/s is reduced under SM-DTFC compared to Optimal DTFC. Moreover, a reduction in thrust force oscillations under SM-DTFC compared to PI-DTFC and Optimal-DTFC can also be observed from Fig. 7(a)–(c) when the speed settles at 600 mm/s.

The magnified views of the speed response of the linear PMSM under the PI-DTFC, Optimal-DTFC, and SM-DTFC during the speed reversal transient are compared in Fig. 8. It is evident from Fig. 8 that the speed response under SM-DTFC is 10% faster when compared to that of PI-DTFC. However, in comparison to Optimal-DTFC, the speed response of SM-DTFC during speed reversal is slightly faster.

It can be observed from Table II that the IAE index for the speed error during speed reversal is in smallest for SM-DTFC compared to PI-DTFC and Optimal-DTFC, which validates the effectiveness of the proposed SM-DTFC.

The steady-state performance of the prototype linear PMSM at 600 mm/s from 0.95 to 1.15 s under the PI-DTFC, Optimal-DTFC, and SM-DTFC is also compared. In order to illustrate the comparison of steady-state performances of the two control schemes, the magnified view of the speed response, flux response, and thrust force response, for PI-DTFC, Optimal-DTFC, and SM-DTFC during the steady state are shown in are shown in Fig. 9(a)–(c), respectively.

Fig. 9 demonstrates that under SM-DTFC, the steady-state low frequency oscillations in speed, thrust force, and stator flux have significantly reduced compared to PI-DTFC and Optimal-DTFC.

The steady-state speed response under PI-DTFC exhibits low-frequency oscillations due to complex friction dynamics of the linear PMSM. These steady-speed oscillations under PI-DTFC also cause oscillations in the force response. The oscillations are not as significant with Optimal-DTFC and SM-DTFC. The quantitative results for steady-state performance of PI-DTFC, Optimal-DTFC, and the SM-DTFC at 600 mm/s and 52 N (average force) in terms of percent flux ripple $\lambda_{\text{rip}}(\%)$, percent force ripple $F_{\text{rip}}(\%)$, and percent speed ripple $v_{\text{rip}}(\%)$ are summarized in Table III. In this analysis, $\lambda_{\text{rip}}(\%)$, $F_{\text{rip}}(\%)$, and $v_{\text{rip}}(\%)$ are given by the following equations:

$$\lambda_{\text{rip}}(\%) = \frac{\sqrt{\frac{1}{N}\sum_{i=1}^{N}\left(\lambda_s(i) - \lambda_{av}\right)^2}}{\lambda_{av}} \times 100 \tag{58}$$

$$F_{\text{rip}}(\%) = \frac{\sqrt{\frac{1}{N}\sum_{i=1}^{N}\left(F_T(i) - F_{av}\right)^2}}{F_{av}} \times 100 \tag{59}$$

$$v_{\text{rip}}(\%) = \frac{\sqrt{\frac{1}{N}\sum_{i=1}^{N}\left(v_m(i) - v_{av}\right)^2}}{v_{av}} \times 100 \tag{60}$$

where λ_{av}, F_{av}, and v_{av} represent the average steady-state flux, thrust force, and mover's speed, respectively, and $\lambda_s(i)$, $F_T(i)$,

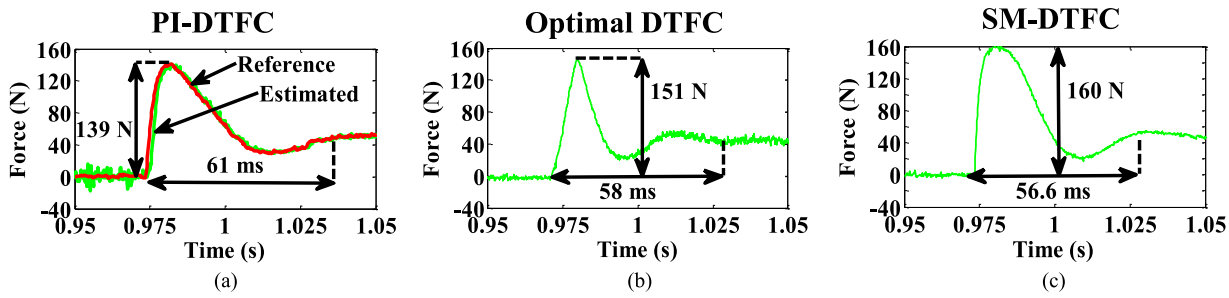

Fig. 6. Magnified thrust force response during startup. (a) PI-DTFC. (b) Optimal-DTFC. (c) SM-DTFC (experiment).

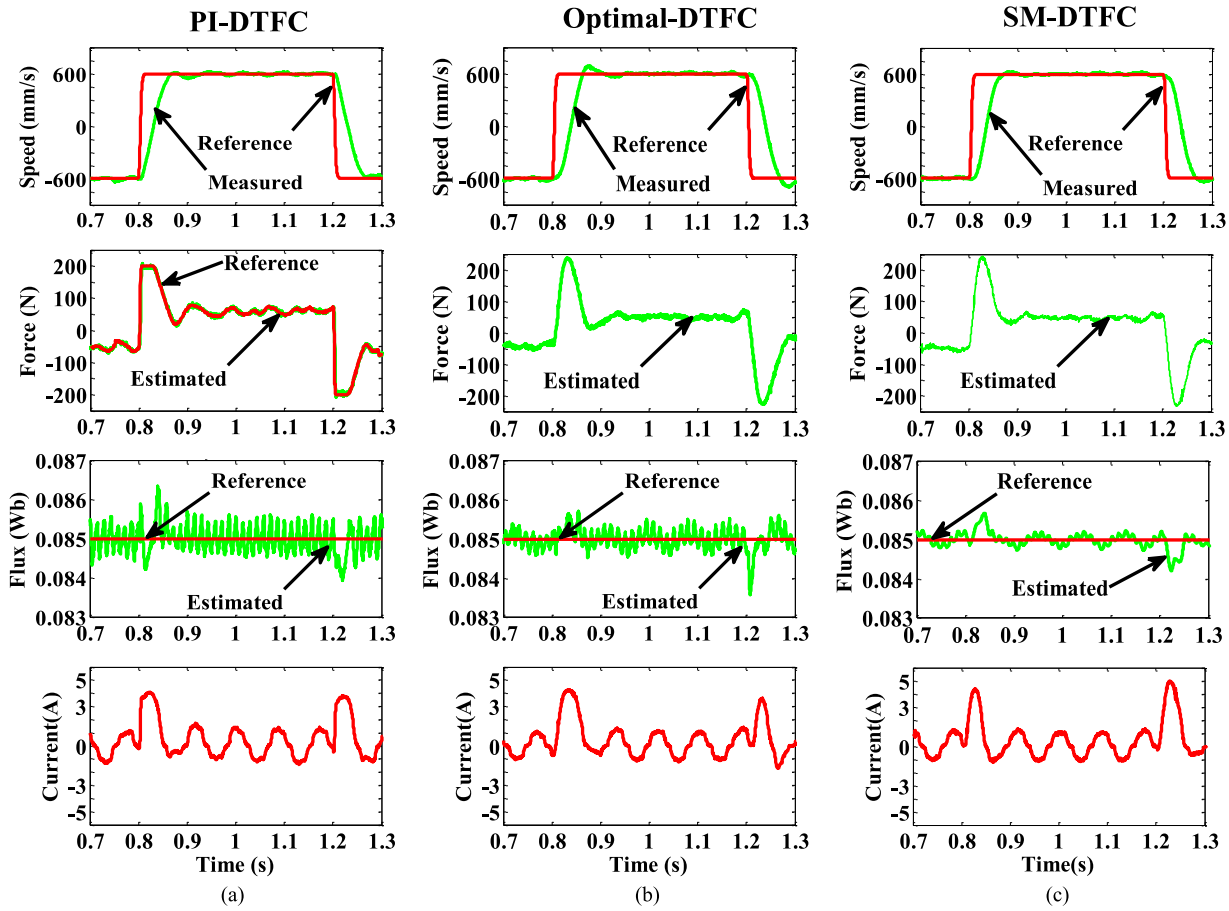

Fig. 7. Speed reversal from –600 to 600 mm/s and steady-state response at 600 mm/s. Speed, force, flux, and stator phase a current responses are shown. (a) For PI-DTFC. (b) For optimal-DTFC. (c) SM-DTFC (experiment).

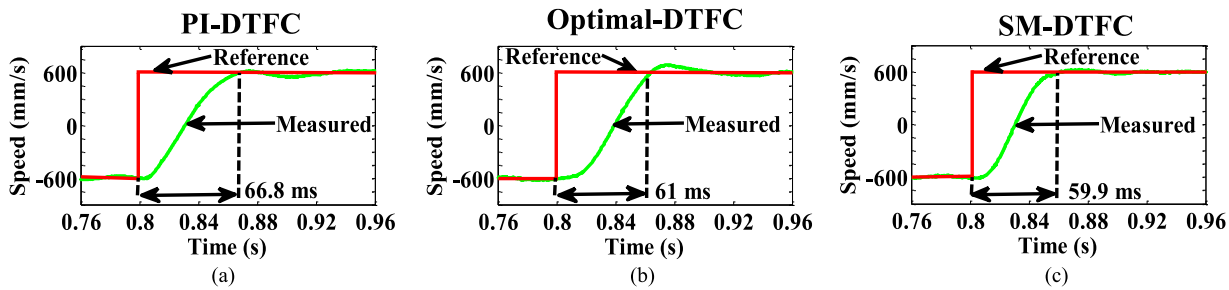

Fig. 8. Magnified view of the speed reversal transient. (a) PI-DTFC. (b) Optimal-DTFC. (c) SM-DTFC (experiment).

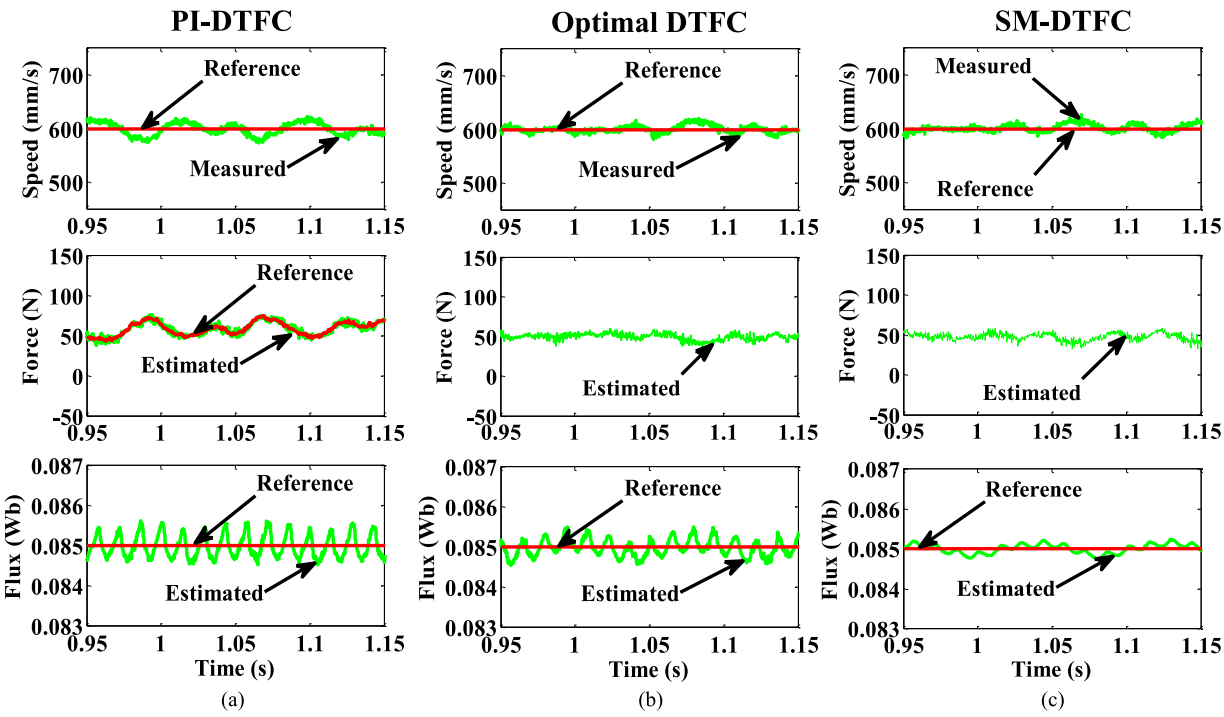

Fig. 9. Steady-state performance at 600 mm/s. Speed, thrust force, and stator flux responses are shown. (a) PI-DTFC. (b) Optimal-DTFC. (b) SM-DTFC (experiment).

TABLE IV
COMPARISON OF RISE TIME OF PI-DTFC, OPTIMAL-DTFC, AND SM-DTFC WITH VARIATION IN R_s

Type of transient phenomena	Parameter Value	Rise Time (s)		
		PI-DTFC	Optimal-DTFC	SM-DTFC
Start up 0 to 200 mm/s	R_s (Nominal)	35.2	31.0	30.0
	0.66 R_s	38	33.2	31.1
	0.5 R_s	41	35.4	33.7
Start up -600 to 600 mm/s	R_s (Nominal)	66.8	61.0	59.9
	0.66 R_s	69.1	65.8	63.9
	0.5 R_s	72.6	70.0	67.3

TABLE V
COMPARISON OF RISE TIME OF PI-DTFC, OPTIMAL-DTFC, AND SM-DTFC WITH VARIATION IN L_s

Type of transient phenomena	Parameter Value	Rise Time (s)		
		PI-DTFC	Optimal-DTFC	SM-DTFC
Start up 0 to 200 mm/s	L_s (Nominal)	35.2	31.0	30.0
	0.66 L_s	40.5	34.7	32.7
	0.5 L_s	44.1	37.9	35.3
Start up -600 to 600 mm/s	L_s (Nominal)	66.8	61.0	59.9
	0.66 L_s	73.7	70.1	67.6
	0.5 L_s	82.4	79.2	73.0

and $v_m(i)$ are the instantaneous values of flux, thrust force, and mover's speed. N is the number of samples.

It can be observed from Table III that the SM-DTFC reduces the percentage ripple in steady-state speed, stator flux, and thrust force response compared to PI-DTFC, which validates the superior steady-state performance of the proposed SM-DTFC.

C. Evaluation of Robustness to the Parameter Variation

The performance of the proposed SM-DTFC subject to variations in stator resistance R_s and inductance L_s is experimentally evaluated and compared to that of PI-DTFC and Optimal-DTFC. Experimental results summarizing the comparison of the performance for these control schemes subject to parameter variation under various operating conditions are provided in Tables IV–VI. The effect of increase in the stator resistance on the rise time of speed response during startup and speed reversal transient for the three control schemes is compared in Table IV. In order to simulate experimentally the effect of 50% and 100% increase in the stator resistance, the controller gains for PI-DTFC, Optimal-DTC, and the proposed SM-DTFC were tuned using the reduced values of 0.66 R_s and 0.5 R_s, respectively for the stator resistance instead of the nominal value of R_s. An identical approach is adopted to experimentally evaluate the effect 50% and 100% increase in the stator inductance L_s on the rise time of speed response for the three control schemes during startup and speed reversals and results are detailed in Table V.

It can be observed from Table IV that the rise time of the speed response during startup and speed reversal increases for PI-DTFC, Optimal-DTFC, and the proposed SM-DTFC when the gains for these control schemes are tuned using reduced

TABLE VI
COMPARISON OF STEADY-STATE PERFORMANCE OF PI-DTFC, OPTIMAL-DTFC, AND SM-DTFC WITH VARIATION IN L_s

600 mm/s, 52 N	Parameter Value	Rise Time (s)		
		PI-DTFC	Optimal-DTFC	SM-DTFC
F_{rip} (%)	L_s (Nominal)	10.48	5.83	5.79
	1.5 L_s	12.3	6.01	5.85
	2 L_s	14.8	6.62	5.98
v_{rip} (%)	L_s (Nominal)	1.92	1.11	1.08
	1.5 L_s	2.17	1.23	1.10
	2 L_s	2.41	1.59	1.17

values of stator resistance compared to the nominal value. However, Table IV demonstrates that the proposed SM-DTFC has the smallest variation in the rise time of speed response during both the startup and reversal operations compared to the other two control schemes. Therefore, a superior robustness performance of SM-DTFC under variation in the stator resistance is evident when compared to that of PI-DTFC and Optimal DTFC. It is also clear from Table V that the SM-DTFC shows a superior robustness considering smaller variation in the rise time of the speed response compared to the other two benchmarked control schemes during startup and reversal when an increase of 50% and 100% in the stator inductance L_s is experimentally simulated.

The effect of variation in inductance on the steady-state speed and thrust for response is also evaluated experimentally for the three control schemes and compared in Table VI. When the controller gains were tuned using a higher value of stator inductance, i.e., $1.5\ L_s$ and $2\ L_s$, the steady-state ripple in speed and thrust force response increased significantly for PI-DTFC and Optimal-DTFC. However, the proposed SM-DTFC demonstrates a minimal deterioration of the steady-state speed and thrust force response in terms of percent ripple when compared to the benchmarks. Therefore, it can be concluded from the experimental results of Tables IV–VI that the proposed SM-DTFC shows the improved robustness under parameter variation when compared to PI-DTFC and Optimal DTFC.

VII. CONCLUSION

A combined speed and direct thrust force control scheme is proposed based on sliding mode control utilizing space vector modulation for the linear PMSM. In order to eliminate the average steady-state tracking error, pure integral action is augmented directly into the control laws by using a modified reachability condition.

The combined dynamic of the mover's speed and thrust force are expressed by a second-order nonlinear SISO system considering the speed and thrust force as states. The sliding surface is formulated in terms of the tracking error in the speed. The formulation of the sliding mode control is performed using a modified reachability condition which allows direct inclusion of pure integral action in the control law to ensure zero average steady-state tracking error in thrust force. A similar approach is utilized to formulate the sliding mode control law to achieve the tracking of the stator flux under the MFPA trajectory. Experimental results clearly indicate that the proposed SM-DTFC scheme exhibits excellent control of flux and thrust force with faster transient response, reduced steady-state oscillations and improved robustness to parameter variation when compared to the state-of-the-art PI-DTFC and Optimal-DTFC.

REFERENCES

[1] I. Takahashi and T. Noguchi, "A new quick-response and high-efficiency control strategy of an induction motor," *IEEE Trans. Ind. Appl.*, vol. 22, no. 5, pp. 820–827, Sep. 1986.

[2] L. Zhong, M. F. Rahman, W. Y. Hu, and K. W. Lim, "Analysis of direct torque control in permanent magnet synchronous motor drives," *IEEE Trans. Power Electron.*, vol. 12, no. 3, pp. 528–536, May 1997.

[3] M. F. Rahman, L. Zhong, and L. Khiang Wee, "A direct torque-controlled interior permanent magnet synchronous motor drive incorporating field weakening," *IEEE Trans. Ind. Appl.*, vol. 34, no. 6, pp. 1246–1253, Nov./Dec. 1998.

[4] F. Niu, B. Wang, A. S. Babel, K. Li, and E. G. Strangas, "Comparative evaluation of direct torque control strategies for permanent magnet synchronous machines," *IEEE Trans. Power Electron.*, vol. 31, no. 2, pp. 1408–11424, Feb. 2016.

[5] K. Yoshida, Z. Dai, and M. Sato, "Sensorless DTC propulsion control of PM LSM vehicle," in *Proc. Power Electron. Motion Control Conf.,* 2000, vol. 1, pp. 191–196.

[6] J. Cui, C. Wang, J. Yang, and D. Yu, "Research on force and direct thrust control for a permanent magnet synchronous linear motor," in *Proc. IEEE Ind. Electron. Conf.*, 2004, vol. 3, pp. 2269–2272.

[7] S. Cheng-Chung and H. Yi-Sheng, "Based on direct thrust control for linear synchronous motor systems," *IEEE Trans. Ind. Electron.*, vol. 56, no. 5, pp. 1629–1639, May 2009.

[8] C. Edwards and S. K. Spurgeon, *Sliding Mode Control: Theory and Applications*. New York, NY, USA: Taylor & Francis, 1998.

[9] V. Utkin, "Variable structure systems with sliding modes," *IEEE Trans. Automat. Control*, vol. 22, no. 2, pp. 212–222, Apr. 1977.

[10] M. A. M. Cheema, J. E. Fletcher, D. Xiao, and M. F. Rahman, "A direct thrust control scheme for linear permanent magnet synchronous motor based on online duty ratio control," *IEEE Trans. Power Electron.*, vol. 36, no. 6, pp. 4416–4428, Jun. 2016.

[11] A. Sabanovic and D. B. Izosimov, "Application of sliding modes to induction motor control," *IEEE Trans. Ind. Appl.*, vol. IA-17, no. 1, pp. 41–49, Jan. 1981.

[12] S. Low, K. J. K. Tseng, T. H. Lee, K. W. Lim, and K. S. Lock, "Strategy for the instantaneous torque control of permanent-magnet brushless DC drives," *Electr. Power Appl. IEE Proc. B*, vol. 137, pp. 352–363, 1990.

[13] T. S. Low, T. H. Lee, K. S. Lock, and K. J. Tseng, "DSP-based instantaneous torque control in permanent magnet brushless D.C. drives," *Mechatronics*, vol. 1, pp. 203–229, 1991.

[14] L. Teck-Seng, L. Tong-Heng, K. J. Tseng, and K. S. Lock, "Servo performance of a BLDC drive with instantaneous torque control," *IEEE Trans. Ind. Appl.*, vol. 28, no. 2, pp. 455–462, Mar./Apr. 1992.

[15] V. Utkin, J. Guldner, and J. Shi, *Sliding Mode Control in Electro-Mechanical Systems*. New York, NY, USA: Taylor & Francis, 2009.

[16] A. Sabanovic, N. Sabanovic, and K. Ohnishi, "Sliding mode in power converters and motion control systems," *Int. J. Control*, vol. 57, pp. 1237–1259, 1993.

[17] A. Sabanovic, "Variable structure systems with sliding modes in motion control—a survey," *IEEE Trans. Power Electron.*, vol. 7, no. 2, pp. 212–223, May 2011.

[18] X. Zhuang and M. Faz Rahman, "Direct torque and flux regulation of an ipm synchronous motor drive using variable structure control approach," *IEEE Trans. Power Electron.*, vol. 22, no. 6, pp. 2487–2498, Nov. 2007.

[19] R. F. Fung, F. J. Lin, and K. W.Chen, "Application of two-phase vsc with integral compensation in speed control of a pm synchronous servomotor," *Int. J. Syst. Sci.*, vol. 21, pp. 1265–1273, 1996.

[20] D. Q. Zhang and S. K. Panda, "Chattering-free and fast-response sliding mode controller," *Control Theory Appl. IEE Proc.*, vol. 146, pp. 171–177, 1999.

[21] B. In-Cheol, K. Kyeong-Hwa, and Y. Myung-Joong, "Robust nonlinear speed control of PM synchronous motor using boundary layer integral sliding mode control technique," *IEEE Trans. Control Syst. Technol.*, vol. 8, no. 1, pp. 47–54, Jan. 2000.

[22] G. Foo and M. F. Rahman, "Sensorless sliding-mode MTPA control of an IPM synchronous motor drive using a sliding-mode observer and HF signal injection," *IEEE Trans. Ind. Electron.*, vol. 57, no. 4, pp. 1270–1278, Apr. 2010.
[23] L. W. Chang, "A MIMO sliding control with a first-order plus integral sliding condition," *Automatica*, vol. 27, pp. 853–858, 1991.
[24] L. W. Chang, "Dynamics of a sliding control with a first-order plus integral sliding condition," *Dyn. Control*, vol. 2, pp. 201–219, 1992.
[25] M. A. M. Cheema, J. Fletcher, M. F. Rahman, and D. Xiao, "Modified direct thrust control of linear permanent magnet motors with sensorless speed estimation," in *Proc. IEEE Ind. Electron. Conf.*, 2012, pp. 1908–1914.
[26] M. A. M. Cheema, J. E. Fletcher, M. F. Rahman, and D. Xiao, "Optimal, combined speed and direct thrust control of linear permanent magnet synchronous motors," *IEEE Trans. Energy Convers.*, vol. 31, no. 3, pp. 947–958, Sep. 2016.
[27] M. A. M. Cheema, J. E. Fletcher, D. Xiao, and M. F. Rahman, "A linear quadratic regulator based optimal direct thrust control of linear permanent magnet synchronous motor," *IEEE Trans. Ind. Electron.*, vol 63, no. 5, pp. 2722–2733, May 2016.
[28] Z. Jun, X. Zhuang, T. Lixin, and M. F. Rahman, "A novel direct load angle control for interior permanent magnet synchronous machine drives with space vector modulation," in *Proc. Int. Power Electron. Drives Syst.*, 2005, pp. 607–611.
[29] Y. Inoue, S. Morimoto, and M. Sanada, "Examination and linearization of torque control system for direct torque controlled IPMSM," *IEEE Trans. Ind. Appl.*, vol. 46, no. 1, pp. 159–166, Jan./Feb. 2010.
[30] T. Sharaf-Eldin, M. W. Dunnigan, J. E. Fletcher, and B. W. Williams, "Nonlinear robust control of a vector-controlled synchronous reluctance machine," *IEEE Trans. Power Electron.*, vol. 14, no. 6, pp. 1111–1121, Nov. 1999.
[31] J. J. E Slotine and S. S. Sastry, "Tracking control of nonlinear systems using sliding surfaces, with application to robot manipulator," *Int. J. Control*, vol. 38, no. 2, pp. 465–492, 1983.
[32] J. J. E. Slotine, "Sliding controller design for nonlinear systems," *Int. J. Control*, vol. 40, no. 2, pp. 421–434, 1984.
[33] J. J. E. Slotine, *Applied Nonlinear Control*. Englewood Cliffs, NJ, USA: Prentice-Hall, 1991.
[34] K. Ohishi, M. Nakao, K. Ohnishi, and K. Miyachi, "Microprocessor-controlled DC motor for load-insensitive position servo system," *IEEE Trans. Ind. Electron.*, vol. IE-34, no. 1, pp. 44–49, Feb. 1987.
[35] J. S. Ko, J. H. Lee, S. K. Chung, and Y. Myung Joong, "A robust digital position control of brushless DC motor with dead beat load torque observer," *IEEE Trans. Ind. Electron.*, vol. 40, no. 5, pp. 512–520, Oct. 1993.

Muhammad Ali Masood Cheema (S'12–M' 16) received the B. Sc. (first class Honors) with two gold medals and M.Sc. degrees both in electrical engineering from the University of Engineering and Technology, Lahore, Pakistan, in 2008 and 2012, respectively, and the Ph.D. degree in electrical engineering from the University of New South Wales (UNSW), Sydney, NSW, Australia, in 2016.

He is currently leading the research and development at the Northern Transformer, Inc., Maple, ON, Canada. He is also contributing toward the development of advanced nonlinear control schemes for multiphase machines in the energy system research group at UNSW, Australia, as a visiting fellow. His research interests include power electronics, electrical drives, nonlinear control, and electric machine design.

John Edward Fletcher (M'11–SM'13) received the B.Eng. (first class Honors) and Ph.D. degrees in electrical and electronic engineering from Heriot Watt University, Edinburgh, U.K., in 1991 and 1995, respectively.

He is currently a Professor with the University of New South Wales, Sydney, NSW, Australia. His research interests include distributed and renewable integration, pulsed-power applications of power electronics, and the design and control of electrical machines.

Mohammad Farshadnia (S'11–M'16) received the B.Sc. and M.Sc. degrees in electrical engineering from the University of Kashan, Kashan, Iran, in 2008 and 2011, respectively, and the Ph.D. degree in electrical engineering from the University of New South Wales, Sydney, NSW, Australia, in 2016.

He is currently with the Energy Systems Research group, University of New South Wales. His research interests include multiphase PM machines, electromagnetics and drive systems, and renewable energy.

Muhammad Faz Rahman (F'14) received the Bachelor of Electrical Engineering degree (first class Honors) from Bangladesh University of Engineering and Technology, Dhaka, Bangladesh, in 1972, and the M. Eng. and Ph.D. degrees from the University of Manchester Institute of Science and Technology, Manchester, U.K., in 1975 and 1978, respectively.

He is currently a Full Professor with the University of New South Wales, Sydney, NSW, Australia. His research interests include electrical machines, drives, and power electronics.